Surface-tension-gradient-induced flow in freely suspended liquid crystalline films

M. I. Godfrey and D. H. Van Winkle
Department of Physics and Center for Materials Research and Technology, The Florida State University, Tallahassee, Florida 32306-3016
(Received 25 September 1995)

Flow was created in freely suspended liquid crystal films (FSLCFs) in the smectic-*C* phase using gradients in the surface tension to drive the motion. The director field was distorted into a pattern of vortices which wind upon themselves while a temperature gradient was applied. A dependence of the pattern in the director field on the topological defects of index $s=+1,0$, or -1 that are isolated in the vortex of the flow was observed. The flow pattern for the $s=-1$ defect has not been observed in FSLCFs with other flow fields. The diffusion constant for the $\hat{c}$-director orientation is extracted from the orientation field patterns under flow and is compared to other independent measurements. The Schlieren pattern of the $\hat{c}$-director field will be shown to arise from the coupling between the fluid velocity and director orientation and will also be shown to be mediated by the topological index of the defect through the use of a model of the dynamical equations of a two-dimensional nematic. [S1063-651X(96)05708-X]

PACS number(s): 61.30.−v, 47.15.−x

I. INTRODUCTION

Freely suspended liquid crystal films (FSLCFs) have been extremely rich systems for study since their rediscovery nearly 20 years ago [1]. They have one of the largest free surface to volume ratios of any physical system, the phase diagram of the liquid crystal is changed from that of the bulk, and in some ways the films behave as real two-dimensional systems [2]. The smectic-*C* phase of such films is particularly amenable to study since depolarized microscopy may be used to visualize the two-dimensional orientation field of the tilted molecules. Many experiments have been performed studying the changes in the orientation field in response to electric, magnetic, and shear fields. We have studied the nonequilibrium dynamics of FSLCFs undergoing flow induced by thermal gradients.

Smectics are layered liquid crystal phases, where the molecules are orientationally ordered and the density of molecular centers is modulated in one direction. The presence of both orientational and positional order makes the hydrodynamics of smectics generally complex [3,4]. Upon spreading a smectic into a film, the free surfaces (top and bottom) define nodes in the density wave. Only an integral number of layers may exist between these nodes. The films are quantized in thickness to the number of smectic layers present. If a shear force is applied, the film will flow in response. Since the thicknesses of FSLCFs are typically less than the wavelength of light, the observable flow response is only parallel to the plane. Thus the film can be modeled as a two-dimensional fluid. This simplification in the flow behavior has been used to study the hydrodynamics of smectic-*A* and smectic-*C* films [5,6].

There is a well-defined average tilt angle ($0 \leqslant \theta < 30°$) of the molecules with respect to the wave vector of the density modulation. For a smectic-*C* (Sm-*C*) film, the projection of the average orientation of the molecules in the layer plane defines the $\hat{c}$ director. It expresses the average local azimuthal orientation of the molecules in the layer. The orientation of the $\hat{c}$ director may be visualized in depolarized reflection microscopy [1,7].

An earlier study allowed for the indirect observation of the effects of the flow field on the orientation field's topology by mechanically shearing the FSLCF [6]. A Sm-*C* film was made to flow in two dimensions by rotating a pin which penetrated the film. The pin was removed to study the relaxation of the flow. Both a phase-winding state and a flow-alignment state were observed for the orientation field response.

In this paper we describe a shear flow experiment in FSLCFs driven by thermally induced surface-tension gradients along the outer edges of the film. There is no internal boundary. The inducing shear forces for the flow are created thermally rather than mechanically. Consequently, the flow velocity profiles are different from earlier experiments. Two flow vortices, showing rotational flow, are created by vorticity diffusion from the film edges. It was possible to directly observe the interaction of the topological defects with the flow, and to observe the effect of a defect with a topological index of $s=-1$ on the flow-orientation patterns. The observations of the interaction of the flow vortex with single defects of topological index $s=1,0$, and -1 are described. The relationship between the observed patterns and the interaction of the flow with the orientational field defects is outlined in a simplified model of the dynamics of these systems.

II. EXPERIMENT

The material used was a racemic mixture of decyloxybenzyalidene anline methyl butyl cinnamate (DOBAMBC), which exhibits a Sm-*C* phase between 76 °C and 96 °C [8]. Observations were also made with the room temperature Sm-*C** mixture ZLI-3232, available from E. Merck Chemicals. These observations agreed qualitatively with the results from the DOBAMBC samples.

In this work, FSLCFs were created by mechanically drawing a small amount of the smectic liquid crystal across a rectangular aperture in a clean steel shim or in aluminum

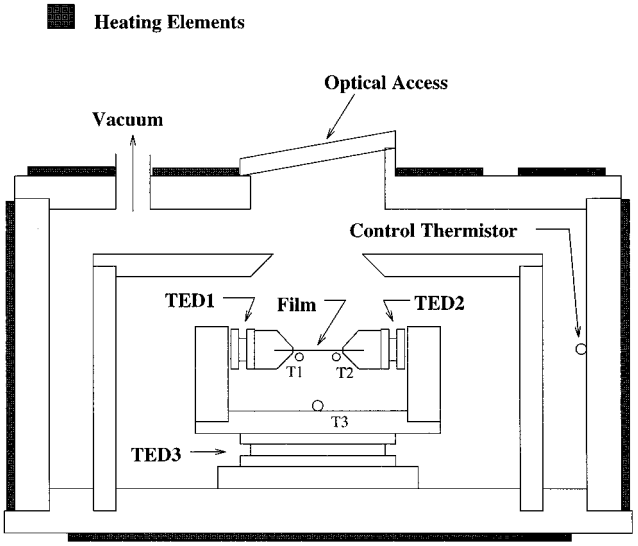

FIG. 1. Thermal enclosure. The films were created in the center of an evacuated, thermally controlled chamber on a steel substrate suspended between two copper blocks. The blocks were attached to thermoelectric heaters (TED1 and TED2) whose heat output was monitored by two thermistors ($T1$ and $T2$). A third thermoelectric heater and thermistor (TED3 and $T3$) maintained the gradient stage at an average temperature. The control thermistor was used to monitor the overall temperature of the oven, with the heating elements providing the necessary thermal power to the oven walls.

foil. The steel shims were approximately 0.25 mm in thickness with apertures which were mechanically milled from them. The aluminum foil substrates were about 0.03 mm in thickness, were cut using an Nd-YAG laser (YAG denotes yttrium aluminum garnet), and mounted on a frame for mechanical support. For both substrates, the holes had aperture ratios between 1:2 and 1:10, with the short side typically 2 mm in length.

An oven was constructed to elevate and maintain the average temperature of the FSLCF. The oven's structure served to isolate the FSLCF from mechanical vibrations and thermal fluctuations in the laboratory, while still allowing mechanical, electrical, and optical access to the oven's interior. A schematic cross section of the oven is presented in Fig. 1.

The FSLCFs were created on a thermal gradient stage that was placed within the oven. The gradient stage was used to apply and maintain a constant temperature difference across the steel shim holding the film. The rectangular apertures of the film holders were mounted with the short sides of the aperture parallel to the direction of the applied thermal gradients. The two thermoelectric heat pumps used to create the thermal gradient generated additional heat. A third thermoelectric heat pump connected the thermal gradient stage to the outside wall of the oven. This was used to transfer excess heat onto the outside wall, where it dissipated into the cooler environment of the laboratory. The average temperature of the oven was typically maintained at a constant, intermediate level between the extremes imposed by the gradient control.

The laser illuminating the film could be used to induce flow. The films were too thin to be directly heated by the laser radiation [9]. However, if the Gaussian intensity profile of the spatially filtered laser beam impinged on the edge of

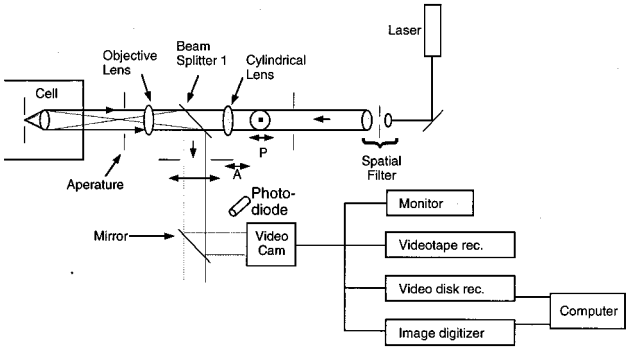

FIG. 2. Optical setup for a depolarized reflection microscope.

the metal frame holding the film, flow occurred on the film. Using the laser beam for heating did not allow for sensitive control of the applied temperature gradient. For this reason, for most experiments direct heating of the film holder's substrate by thermoelectric heat pumps was used.

It was necessary to eliminate the air surrounding the film. In the presence of an overlying atmosphere the thermally induced flow in the film could be dominated by the convective flows of the air mass above the film. Reducing the air pressure within the cell dropped the Rayleigh number for the vapor below its critical value necessary for the onset of convection in air. The critical Rayleigh number for these slip conditions is 657.6 [10]. At atmospheric conditions, for a temperature difference of 5.0 °C in a volume of about 1.0 cm^3 and an ambient temperature of 100 °C, the Rayleigh number for air in the chamber will be about 1000. Reducing the air pressure below 1 torr will reduce the Rayleigh number for the gas 100-fold, thereby decoupling the action of the air motion on the film's surfaces. The reduced air pressure also lowered the conductive capacity of the air mass, further decoupling thermal flows between the air mass and film. The cell was evacuated to a pressure below 1 torr, which was still substantially above the typical vapor pressures of liquid crystals. Mechanical access into the oven was provided to spread the films while under this partial vacuum.

The $\hat{\vec{c}}$-director orientation field was observed using depolarized reflection imaging (see Fig. 2). Video recordings of the depolarized images of the film were made for later analysis of the evolution of the orientation field under the applied gradients. The orientation field was observed as a Schlieren texture under reflected depolarized light (see the photographs in Figs. 9–11). The reflected intensity viewed through an analyzer crossed with respect to the polarization of the incident light varied as

$$I = I_0 \sin^2 \Phi, \tag{1}$$

where Φ is the local polar orientation of the $\hat{\vec{c}}$ field [7]. The Schlieren texture provides direct measure of the relative orientation of the $\hat{\vec{c}}$ director.

Films of uniform thickness were required in order to model the system as a two-dimensional fluid. When the smectic liquid crystal was spread across the aperture in the film holder, the initial film typically was not uniform in thickness. The films were allowed to anneal over a period of

several hours in the Sm-*A* phase to achieve a uniform thickness before reducing the temperature to bring it into the Sm-*C* phase. Most of the films used in these experiments ranged in thickness from about 100 layers to 250 layers (0.3–0.8 μm for the material used), and were uniform in thickness across the film's extent. In addition, some very thin films of about three layers in thickness were also created and used to compare our results with previously obtained results.

Any constant orientation boundary condition at the edge of the film will lead to a defect in the orientational field within the body of the film. The boundary must be a closed circuit enclosing the body of the film. The orientation field must then continuously rotate as the closed circuit is traversed in order to maintain locally the constant orientation boundary condition. This translates to a global 2π rotation in the orientation field around the circuit. As long as the boundary circuit is microscopically smooth, that is, it does not contain sharp angles, the orientation field in its vicinity will vary slowly in space. However, at some point within the body of the film, no configuration of the director field will be commensurate with the 2π rotation imposed by the boundary. The orientational ordering is destroyed at that point and a point defect, called a disclination point, is introduced. Since the orientation field undergoes a $+2\pi$ rotation around this point disclination, it is said to have a net $+1$ topological charge. It is also possible for -1 topological charges to exist in the film, where the orientation field undergoes a -2π rotation in a circuit enclosing the incommensurate point. However, it has not been possible to create the boundary conditions necessary for the existence of a net topological charge of -1 in a freely suspended smectic-*C* film. Therefore the presence of a -1 topological charge in a smectic-*C* FSLCF is always accompanied with the presence of a balancing $+1$ disclination elsewhere in the film. Under optical observation, uniform Sm-*C* films would contain one or more point disclinations, either moving freely about the film or anchored to the edge of the film holder. The film holder's edges were not treated in any special way other than being cleaned thoroughly after the aperture was either milled or laser cut out of the substrate.

As in all fluids, there is no direct measure of the velocity of flow. Flow was monitored by observing the motion of objects on the film surface or the change in the Schlieren pattern associated with the orientation field. Moving objects included dust motes and islands of liquid crystal, both of which alter the flow of the film. The flow field always affects the Schlieren pattern, but the pattern does not always move with the fluid velocity.

III. RESULTS

We report initiation of flow via an applied thermal gradient, the measurement of the resulting flow velocities, and the observation of three static orientation patterns in the presence of the flowing fluid. In the analysis section these results are understood by applying the Ericksen-Leslie equations in two dimensions.

A series of experiments were performed to verify that a thermal gradient was, by itself, sufficient to cause flow in FSLCFs. First, a vertical geometry flow in the films was seen in response to heating a portion of the film holder. Next, in the horizontal geometry of the film oven, the laser was focused on the film holder and rapid flow was seen. This laser-heating-induced flow was directed from the cooler outer edges of the Gaussian beam profile into the hotter central region. The induced, nonuniform thermal gradients were established on the film through conduction across the film-holder boundary onto the film's surfaces. Finally, a series of careful experiments were performed by creating stable, measured gradients using the thermoelectric devices (TEDs) on the gradient stage in the oven.

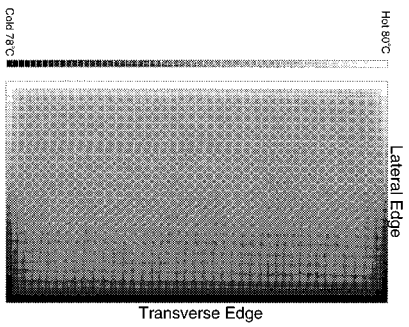

FIG. 3. Temperature profile in one layer of the film as calculated using an iterative relaxation algorithm. The map of temperatures is on the right and the temperature scale is keyed in the column on the left. Temperature at the edge boundaries was set to reflect the temperature gradients on the film holder. The top and bottom surfaces were treated as radiative surfaces. Only conductive and radiative heat transport were considered in the films.

Stable thermal profiles could be created with the TEDs for gradients greater than 0.25 °C/cm. The semiconductive nature of the TEDs defined a bias voltage at which current began to flow through the device. The need for a bias voltage and the fixed separation between the TEDs did not allow for stable gradients below 0.25 °C/cm. The applied gradients on the film holder ranged from about 0.25 °C/cm to 5.00 °C/cm with the gradient control to within ± 0.06 °C/cm. For all gradients applied, flow was observed. Thus, if there is a critical gradient for onset of flow, it is less than 0.25 °C/cm. The temperature profile along the long edges of the aperture, that is, perpendicular to the center line of the shim along which the gradient was applied, was measured. A gradient on the order of 0.02 °C/cm was found. The hottest point on the hot side and the coldest point on the cold side of the aperture were always on the midline of the film holder.

The measured temperatures along the edges of the film were used as the boundary conditions in a computer program used to model the temperature profile of the films. Figure 3 shows a temperature profile calculated for a five layer film. The program modeled the effects of conduction and radiation on the film's thermal profile. An iterative relaxation algorithm was used. The simulation shows radiative cooling produces a region of very uniform temperature in the central areas of the film. The combination of conduction and radiation produces sharp gradients in the temperature close to the edges.

When flow occurs, two counter-rotating, closed vortices form. The geometry of these vortices in the film is indicated in Fig. 4, along with the coordinate axes and the film dimensions used in the analysis of our results. The vortices, as

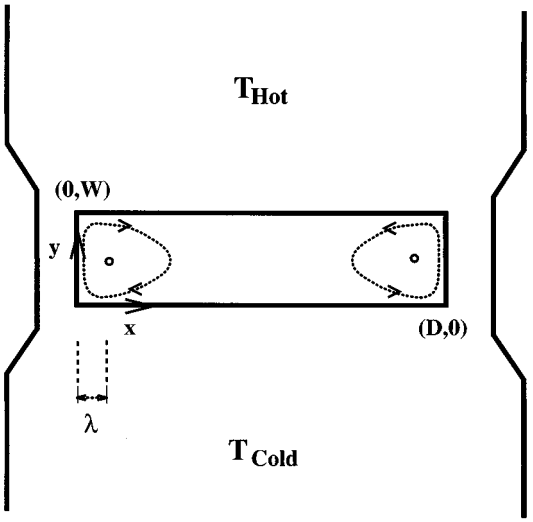

FIG. 4. Schematic of the film holder. D is the length and W the width of the aperture on which the free films were suspended. The x and y coordinate axes are shown on the aperture edge. The lateral edges of the film are taken to be those edges parallel to the y axis, and the transverse edges those parallel to the x axis. λ is the distance from the nearest lateral edge to the center of the flow vortex. The dotted loops within the aperture indicate the general shape of the flow vortices. The arrowheads on the loops indicate the observed direction of rotation for the indicated temperature configuration.

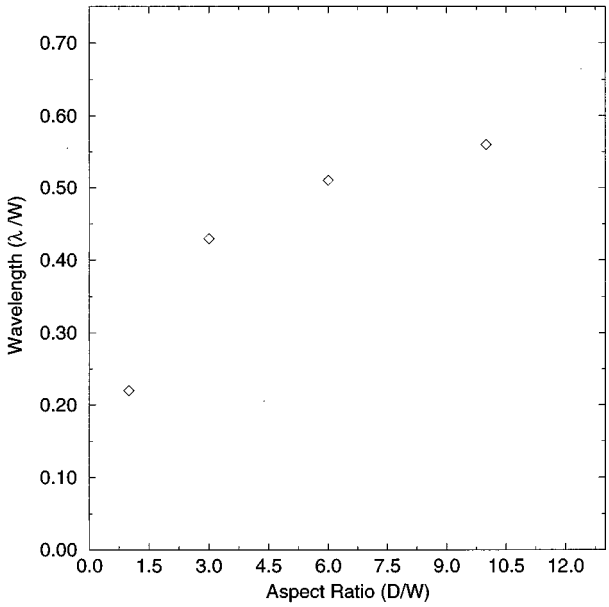

FIG. 5. Aspect ratio vs vortex size. Lengths have been normalized to the width of the film aperture (that is, the lateral length).

delineated by the streamlines, were not circular. They were somewhat elongated and triangular in shape, with the short base of the triangle parallel the short edge of the film aperture. Near this short edge (where the thermal gradient was largest) the flow velocity was largest. In addition, the center of the vortex, defined as that point where the flow velocity was zero, was close to this short edge. The relative sizes of the vortices were measured by the displacement λ of the vortex center from the nearest lateral edge of the film holder, scaled to the dimensions of the lateral edge's length W. The vortex size depended on the aspect ratio of the holder (Fig. 5). As the aspect ratio increased, the separation of the vortices also increased, reducing the interaction. The largest velocities in the vortex occurred in the narrow region close to the lateral edges of the film. The lowest velocities occurred in the broad region of the vortex opposite to the lateral edges. Thus, with the reduction of interaction between vortices, they appear to tend to an optimal distance away from the lateral edge to accommodate the flow rate with the increase in aspect ratio.

Figure 6 is a plot of the velocity versus displacement along the perpendicular from the center of the vortex to the edge of the film holder bearing the large thermal gradient. The center of the vortex for this particular example was located at the coordinates (1.39 mm, 1.50 mm) in a 3:1 aspect ratio film holder with a depth of $d=9.30$ mm and a width of $w=3.10$ mm. In the region of the film between about 0.2 mm and 1.0 mm from the center of the vortex, the velocity increases linearly with displacement. Thus the angular velocity ω of the flow with respect to the vortex center is independent of the radial distance from the center of the vortex r for most of the region between the center of the convective cell and the edge of the substrate. Close to the edge of the film holder, boundary effects dominate, and the velocity rapidly drops to zero, consistent with no-slip boundary conditions.

The functional form of the velocity versus distance from the vortex center has a linear range for other cross sections of the vortex. The slope, however, varies (see Fig. 7, for example). Though the angular velocity ω is independent of r along any given radial line, it is not independent of θ. A plot of the measured angular velocity as a function of θ is given in Fig. 8. This general pattern of the films' cores rotating as

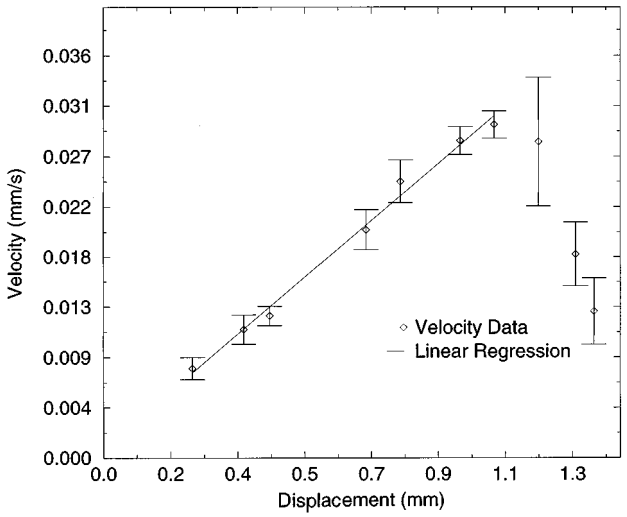

FIG. 6. Velocity profile from the differentially heated edge to the center of the flow vortex. Data are for a three layer thick, smectic-C film, in a 3:1 aspect ratio holder of width $W=9.3$ mm and depth $D=3.1$ mm. Location of the vortex center was at (1.39 mm, 1.50 mm). The cold side was held at 75.0 °C and the hot side held at 76.0 °C over a 9 mm separation.

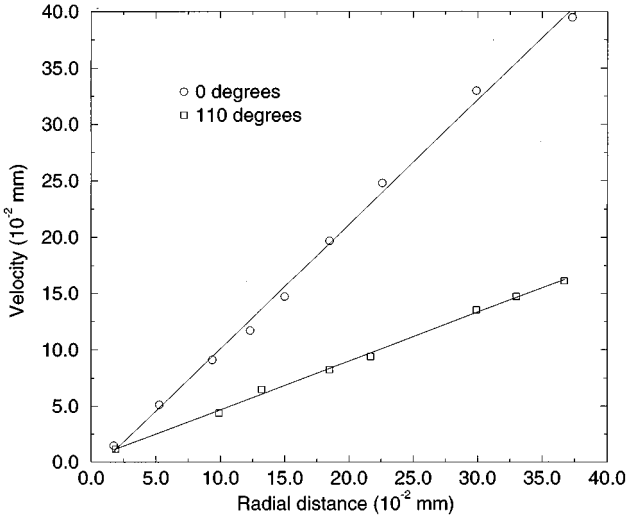

FIG. 7. Velocity profiles through the linear region for two different regions of the vortex flow for the same film illustrated in Fig. 6. $\theta=0$ corresponds to a profile from the center of the vortex to the differentially heated edge. $\theta=110$ corresponds to profile from the center of the vortex to one of the long edges, 110° in the direction of the vortex rotation from the first profile.

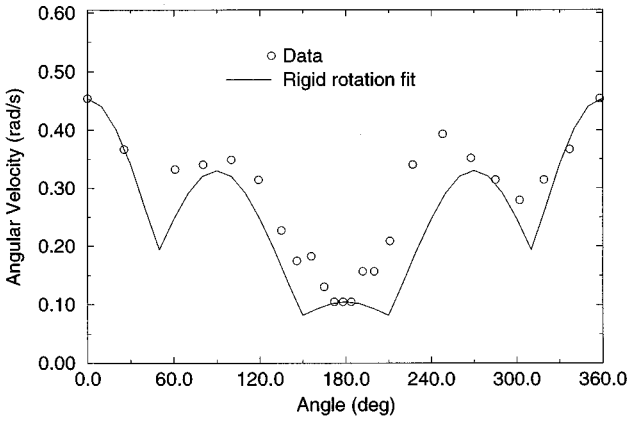

FIG. 8. Angular velocity profile around the center of the flow vortex. Film was 140 layers thick, with a gradient of 81.13 °C −79.70 °C over 8 mm. Center of flow in one vortex was located at (0.70 mm, 0.80 mm). Symbols correspond to data. The line corresponds to a body rotating rigidly, but with a dilatational motion in the radial direction.

a semirigid body was seen for all films, independent of film thickness and aspect ratio, although the location of the vortex center was seen to depend on the aspect ratio. The maximum angular velocity for these films was kept well below 0.50 rad/s. Above this angular velocity, instability in the orientation field was observed, with a $+1$ point disclination located in the center of the vortex becoming unstable and moving out from its stable position in the center of the vortex into the vortex flow itself. The relationship between the maximum fluid velocity and film thickness could not be examined due to the lack of reliable data on the velocity field for very thin films.

Distortions in the Schlieren pattern are always seen with the initiation of flow. Complex and often unstable patterns were commonly observed. Typically, these patterns contained more than one disclination in the core region of the flow vortex, had either isolated plateaus of thicker material or dust motes aggregated in the core, or had point disclinations outside of the core region, either in the flow or anchored to the edges of the film holder.

Three particular patterns stabilized in some films after the initial transients in the flow and orientation field passed. All three of these canonical forms included two regions in the orientation field where the patterns in the Schlieren texture were qualitatively distinct. One region included the area surrounding the center of the vortical motion. The second region was a narrow band outside this core along the edges of the film and along the boundary with the opposing vortex in the film. Each of the stable flow-orientation patterns had a characteristic texture associated with the core and outer region. These are illustrated in Figs. 9–11. We have labeled the three characteristic patterns that we observed in the vortices as ring, spiral, and antispiral.

(1) *The ring regime* (see Fig. 9). The core region is free of disclinations and the brushes in the outer region are closed on themselves, forming rings or, as they are also known, disclination walls [7].

(2) *The spiral regime* (see Fig. 10). A single -1 point defect occurs in the core region of the film, with four brushes emerging from the disclination under crossed polarizers. The brushes spiral outward around the central defect turning in the direction of the flow.

(3) *The antispiral flow regime* (see Fig. 11). A single $+1$ point disclination occurs in the core region, but now the brushes emerging from the disclination are turned away from the flow direction and spiral around the central disclination against the direction of flow.

Various combinations of these three static patterns have been observed to coexist in neighboring counter-rotating vortices. The antispiral pattern has been seen in conjunction with either spiral flow or ring flow in the second vortex. A spiral orientation pattern paired with an antispiral pattern appears to occur only when there are at least three defects on the film. For the observed static patterns one defect remains pinned at the edge of the film and does not affect the general flow pattern. The spiral pattern and the antispiral pattern can occupy neighboring vortices if a $+1$ defect is anchored to the edges of the film, thus maintaining a net topological charge of $+1$. We have also seen a -1 disclination trapped on the edge of the film, allowing two $+1$ defects to be isolated in the core of the flow, resulting in the coexistence of two antispiral patterns.

IV. ANALYSIS

For the FSLCFs, three sets of variables are significant in determining the hydrodynamic behavior of the fluid. These are the temperature, the velocity, and the director. We assume the fluid is incompressible, so that mass conservation is expressed as

$$\vec{\nabla}\cdot\vec{v}=0, \tag{2}$$

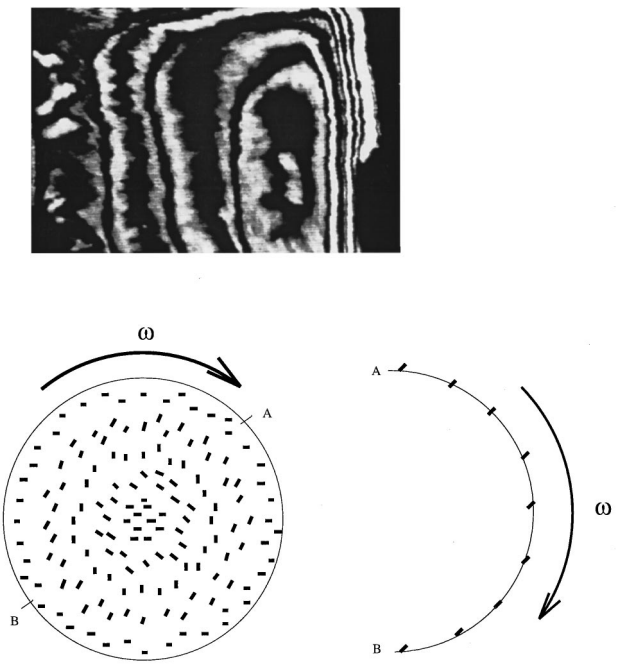

FIG. 9. Ring flow, including a photograph, a schematic of the orientation close to the center of the flow, and a schematic of the local orientation relative to the circumferential (and flow) direction between the points A and B. The photograph is of a film of 120 layers in thickness, in a 6:1 aspect ratio holder with dimensions 0.940 cm by 0.145 cm, and with an applied gradient of 60.3 °C − 59.0 °C, in the smectic-I phase. The photograph covers an area of 0.145 cm × 0.102 cm.

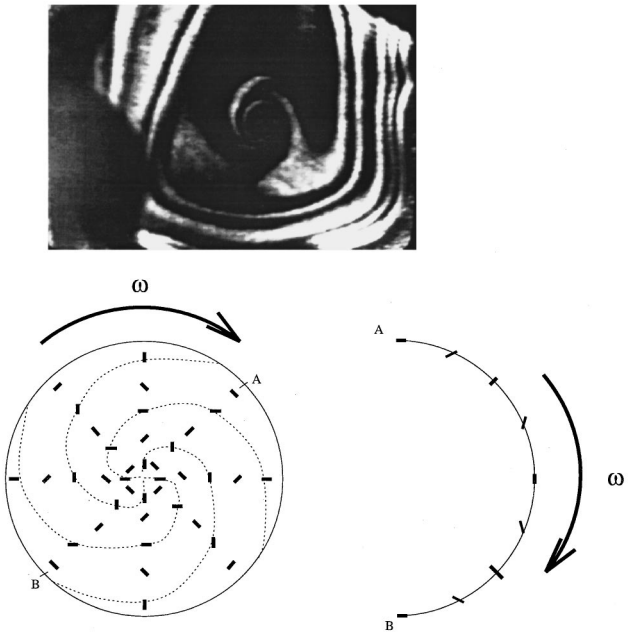

FIG. 10. Spiral flow, including a photograph, a schematic of the orientation close to the disclination, and a schematic of the local orientation relative to the flow circumferential (and flow) direction between the points A and B. The photograph is of a film of 140 layers in thickness, in a 6:1 aspect ratio holder with dimensions 0.940 cm by 0.145 cm, and with an applied gradient of 81.3 °C − 79.7 °C, in the smectic-C phase. The photograph covers an area of 0.145 cm × 0.102 cm. The darker region in the lower right corner is the result of a slight buckling of the film's surface due to an inhomogeneity in the film holder.

where $\vec{v}$ is the fluid velocity. For the remaining equations, it has been shown that the forms of the hydrodynamic equations for a Sm-C film for flow parallel to the plane of the film's surfaces are isomorphic with those of a two-dimensional nematic [11]. Thus the Ericksen-Leslie equations of a nematic [12,13], appropriately reduced to two dimensions, describe the hydrodynamic flow and the induced patterns in films.

In what follows, the equation for the temperature and the equation for the velocity are both approximated by their isotropic forms, without any director dependence. As such, they reduce to a two-dimensional representation of the Navier-Stokes equations for the temperature and velocity. The isotropic forms are shown below along with the boundary conditions on the film and the validity of the approximation is briefly discussed. The coupling between the velocity field $\hat{\hat{v}}$ and director $\hat{\hat{n}}$ is a well-known phenomenon in nematic liquid crystals [12]. The coupling of the director to the velocity field in FSLCFs in the Sm-C phase seen in our experiments is discussed in terms of a two-dimensional nematic model. The relationship between this theory and our experiment are discussed at the end of this section.

A. Equations of motion

The temperature is assumed to be a two-dimensional function. Away from the edges of the film, the temperature $T(z)$ will rapidly equilibrate because of the thinness of the films in the $\hat{\hat{z}}$ direction. As was the case with the viscosity in the momentum equation, only one constant will contribute to the thermal conductivity as a result of the isotropy in the plane of the Sm-A films. The temperature equation is then of the form [15]

$$\frac{\partial T}{\partial t}+(\vec{v}\cdot\vec{\nabla})T=\kappa\nabla^2 T, \tag{3}$$

where T is the temperature and κ is the thermal diffusivity. The gradient operator $\vec{\nabla}$ is two dimensional, with components in the directions of the smectic layering only.

For the velocity equations, the smectic films are assumed to be thin, layered films, with strong shear coupling between the layers, but with the condition that v_z is zero everywhere. The free surfaces do not vary in position nor does the fluid velocity have a component perpendicular to the film's surfaces. Permeation [16], undulation [17,18], or other distortions of the layers and their spacing are therefore assumed to be small and are ignored. In fact, permeation effects between smectic layers have been shown to have effective viscosities an order of magnitude larger than the ordinary in-plane viscosities [16,19,20]. This sluggishness perpendicular to the layers prevents the film from accommodating flow along the layer normal. Energy will be more readily transported parallel to the layering than perpendicular to it. Therefore, in the horizontal FSLCFs, flow along the film's layering direction is easily induced thermally without also inducing a vertical convective motion. If the layer normal lies along the $\hat{\hat{z}}$ direction, then

$$\vec{v}\cdot\hat{\vec{z}}=0. \tag{4}$$

However, the boundary conditions may require $\partial\vec{v}/\partial z\neq 0$, in order to bring the inner layers of the fluid into motion. The variation will be small compared to the changes in velocity over the length of the film. Only xy spatial scales that are much larger than the film's thickness are observable. The layers act as two-dimensional fluids strongly shear coupled to each other. In addition, the anisotropy of the director field is neglected in the momentum equation. For smectic-A films there is no anisotropy of the director in the xy plane. For smectic-C films we assume negligible flow effects due to the anisotropy.

These two assumptions reduce the smectic equations to a set of quasi-two-dimensional equations isomorphic with the Navier-Stokes equations. The third dimension comes into play only through the action of the boundary conditions on the surfaces of the film. The two-dimensional Navier-Stokes equations are

$$\rho\frac{\partial\vec{v}}{\partial t}+(\vec{v}\cdot\vec{\nabla})\vec{v}=-\vec{\nabla}p+\mu\nabla^2\vec{v}, \tag{5}$$

where ρ is the density, $\vec{v}(x,y,z)$ is the two-dimensional velocity field $(v_x,v_y,0)$, p is the pressure, and μ is the kinematic viscosity. Because of the spatial constraints, μ corresponds to the Leslie coefficient μ_4. The gradient operator $\vec{\nabla}$ has components only in the plane of the smectic layering.

Two sets of boundary conditions apply to the films, one set along the rigid walls of the film holder, and a second set on the free surfaces of the film. The temperature in the substrate and the film are equal at the interface between them, and the velocity of the liquid crystal vanishes at these points,

$$T_w(x=0,D;y=0,W)=T_f(x=0,D;y=0,W), \tag{6}$$

$$\vec{v}(x=0,D;y=0,W)=0, \tag{7}$$

where the subscript w denotes the wall of the substrate and the subscript f denotes the film.

Along the free surfaces of the films, the difference in the viscous stresses at the interface balances the gradient in surface tension, which will depend on the local temperature [21], and the heat flux normal to the surface of the film balances the radiative losses to the walls of the enclosure around the film, which may be expressed as a Steffan-Boltzmann process if one assumes the film and the walls act as ideal blackbodies [22],

$$\mu\partial_z v_\tau=\partial_\tau\sigma, \tag{8}$$

$$-\epsilon\partial_z T_f=\delta T^4. \tag{9}$$

The subscript z signifies the normal component and the subscript τ the tangential component in the plane of the film. The scalar quantity σ is the surface tension. The reduction of the atmospheric pressure in the thermal enclosure where the experiments were conducted allows us to ignore the contribution of the air to the viscous stress balance at the boundaries. The surface tension is assumed to be a linear function of the film's surface temperature [23],

$$\sigma(T)=\sigma_0+\alpha(T-T_0), \tag{10}$$

where α represents the excess surface entropy. In most fluids $\alpha<0$, so that the surface traction is directed from a hot region to a cold region. In liquid crystals, and particularly the smectics, the orientational order at the interface leads to an excess surface entropy. Consequently, there is a reversal in the sign for α, so that $\alpha>0$. The gradient in surface tension is then parallel to the gradient in temperature, positive from cold to hot [24,25]. Typically, for the smectics, $\alpha\sim 0.20$ dyn/cm °C [25].

There are also forces associated with the $\hat{\vec{z}}$ direction normal to the film that involve the surface tension. Namely, the pressure must be balanced across the interface. If there is no movement of material along the normal direction, this condition may be written as [21]

$$\delta p=-\sigma\left(\frac{1}{R_1}+\frac{1}{R_2}\right), \tag{11}$$

where δp is the difference in pressure across the interface, σ is the surface tension, and R_1 and R_2 are the principal radii of curvature of the surface. Thus changes in σ may appear as distortions of the flat film's surface without motion occurring.

Turning next to the director field, the in-plane director field is given by $\hat{\vec{c}}=(c_r,c_\theta)$, where $c_r=\cos(\Phi)$ and $c_\theta=\sin(\Phi)$, and where Φ is the local director orientation, with $\Phi=\Phi(r,\theta,t)$. The twist term in the Frank free energy does not contribute in the two-dimensional case, leaving two constants for the splay and bend elastic energies, k_{11} and k_{33}. This is true in FSLCFs for length scales significantly larger than the thickness [14]. The splay and bend constants are assumed to be equal, $k=k_{11}=k_{33}$.

The director evolution equation can then be written as [13]

$$\rho_1\ddot{\Phi}=\lambda_1\left[\left(\frac{d}{dr}v_\theta(r)+\frac{v_\theta}{r}\right)+\dot{\Phi}\right]+\lambda_2\left(\frac{d}{dr}v_\theta(r)-\frac{v_\theta}{r}\right)\cos(2\Phi)-k\nabla^2\Phi, \tag{12}$$

where λ_1 and λ_2 are viscosity coefficients. The orientation field is seen eventually to settle into a static pattern in our experiments, as long as the point disclinations are isolated in the core of the flow. We therefore drop the time dependence in Eq. (12), so that we end up with the dynamical equation

$$\lambda_1\left[\left(\frac{d}{dr}v_\theta(r)+\frac{v_\theta}{r}\right)\right]+\lambda_2\left(\frac{d}{dr}v_\theta(r)-\frac{v_\theta}{r}\right)\cos(2\Phi)-k\nabla^2\Phi=0. \tag{13}$$

If the form of the velocity field can be determined beforehand, the director equation can then be solved either numerically, or in some cases analytically.

B. Thermal field

Allowing transients to decay away in the temperature field and ignoring the contribution of advection, Eq. (3) then becomes Laplace's equation, $\nabla^2 T = 0$. A computer program was written to find a solution using a simple relaxation algorithm. The boundary conditions on the free surfaces and on the edges of the substrate were given in Eqs. (7) and (9). For the calculated distribution shown in Fig. 3, the temperature on the hot side was taken to be 80.0 °C and the temperature on the cold side was 78.0 °C. A uniform thermal gradient was assumed to be applied on the sidewalls connecting the hot side of the substrate to the cold side. The film was assumed to be centered inside a volume with 79.0 °C walls. The constant ϵ is equivalent to the thermal conductivity divided by the Steffan-Boltzman constant; that is, the film is taken to behave like an ideal blackbody. The thermal conductivity was assumed to be 1×10^{-2} W K^{-1} m^{-1}. The aspect ratio of the holder was taken to be 1:2, and the film was taken to be five layers thick. The distribution shown in Fig. 3 gives an indication of the rapid equalization in temperature for all parts of the film away from the edges.

Thermal effects, therefore, are not significant in the central regions of the FSLCFs because radiative cooling rapidly equalizes any gradients in temperature on the FSLCF's surfaces. However, they are significant along the edges of the film. These edge gradients must be considered in order to understand what causes the flow in the films. The observed flows in the smectic films are shear flows induced in the boundary region between the film holder and the film itself through thermocapillary effects — the temperature field and velocity are indirectly coupled through the boundary conditions on the film. Although the velocity vector and temperature field are two dimensional, the boundary conditions make the problem fully three dimensional.

The rapid equalization translates to sharp thermal gradients on the film's surface, with the central core of the flow in thermal equilibrium with the cell walls. The thermal gradients are most pronounced near the lateral edges. It is assumed that this is the basic state of the film. The presence of the thermal gradients on the edges of the film will create a surface-tension gradient that in turn will induce flow.

The simple conductive and radiative model for the thermal field suggests another simplification in understanding the dynamics of the film. Based on Fig. 3, there are three distinct regions of a film, one close to each transverse edge where the thermal gradient is directed there perpendicular to the film's edges, a second region close to the lateral edges, where the dominant thermal gradient is directed parallel to the film's edges, and the broad central region of the film that is very nearly at a uniform temperature.

Consider first the edges of the film transverse to the applied gradient. Assume the film to be infinitely long in the transverse direction and the applied temperatures on each of the transverse edges of the holder aperture to be constant. The temperature must drop from some maximum T_H on the hot side to a minimum T_C on the cold side. The conductive and radiative temperature model suggests that those drops occur in two sharp steps, each step close to each respective edge (see Fig. 3). The films do not sustain flow in the direction of the thermal gradient.

If there were movement of material in the direction of the thermal gradient, flow could not close (conserving mass). The imposed constraint on the vertical velocity due to the smectic layering, $v_z = 0$, is still assumed valid. As there are no distortions in the thermal field to maintain flow in the $\hat{x}$ direction, the continuity equation then has the form

$$\partial_y v_y = 0 \tag{14}$$

so that $v_y = f(z,t)$. In such a case there cannot be flow closure. This is apparent when one considers the boundary condition on the velocity at the holder edge, namely, $v_y = 0$ at $y = 0$ and at $y = W$. With the constraint that there be no vertical velocity component, that is, no component parallel or antiparallel to $\vec{g}$, the flow cannot occur with the application of a temperature gradient across the film.

The structure of the film near its edges is also significant in understanding the flow that develops. Near the boundary between the film and the film holder, the surface tension alters to accommodate the additional contribution the solid film holder makes to the excess surface entropy. For a smectic liquid crystal film, this difference in the surface tension leads to the creation of a meniscus that may be thought of as a number of terraces or steps placed one over the other near the edge of the film holder [26]. A line tension is associated with each step. Along the transverse edges of the film, the applied gradient is perpendicular to the steps of the meniscus, and on the lateral edges, the applied gradient is parallel to the steps of the meniscus.

If flow does not occur, the surfaces near the film edges must be deformed as a consequence of the change in surface tension to accommodate the large temperature gradients. Vertical rearrangement of material, with new layers forming in the meniscus, can manifest this deformation [see Eq. (11)]. For gradients greater than 5.0 °C/cm, the film is seen to thicken, beginning from the hot edge and spreading gradually across the entire film surface. Convective flow perpendicular to the film's surface is not apparent in any of the film steps as the thick regions spread across the film. It has also been shown that the addition of a step in thickness introduces a line tension onto the film surface, and that the surface tension itself is a function of the film's thickness [26]. Thus the thickening on the film's edges may balance the gradient in surface tension in these areas by forming new steps or by rearranging the steps and allowing the film to gradually thicken from one side.

Along the lateral edges, the gradient in temperature is parallel to the film's edge, rather than perpendicular. Since the gradient in temperature is parallel to the steps of the meniscus, the induced surface tension occurs over a film step of uniform thickness. No line tensions occur to balance the surface-tension gradient, and the surface-tension gradient can induce flow. The Marangoni number parametrizes the thermal gradient applied to the film's surfaces in this region. If the Marangoni number is large, the thermal gradient and surface-tension terms prevail over viscous and conductive terms. The Marangoni number for a 66 Å thick Sm-*A* film was found to be $\sim 10^4$.

Motion of the liquid crystal at the lateral edges is a thermocapillary phenomenon. Movement occurs from the cold to

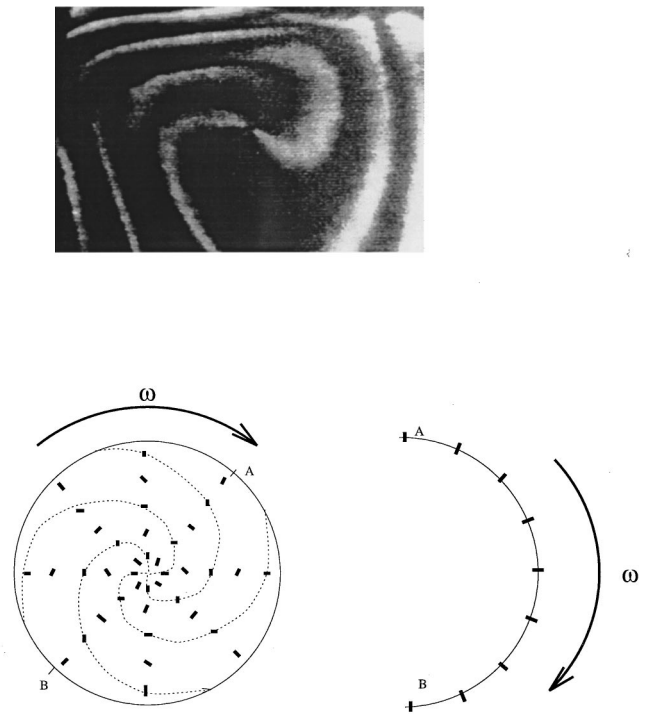

FIG. 11. Antispiral flow, including a photograph, a schematic of the orientation close to the disclination, and a schematic of the local orientation relative to the flow circumferential (and flow) direction between the points A and B. The photograph is of a film of 140 layers in thickness, in a 6:1 aspect ratio holder with dimensions 0.940 cm by 0.145 cm, and with an applied gradient of 81.3 °C −79.7 °C, in the smectic-C phase. The photograph covers an area of 0.145 cm × 0.102 cm. The four brushes are not distinct due to the strong scattering in the thick films that has led to a partial loss of the depolarization component in the scattered light.

the hot end of the gradient. The excess surface entropy α was defined by Eq. (10) to be

$$\alpha = \frac{d\sigma}{dT}, \tag{15}$$

where σ is the surface tension and T is the temperature [see Eq. (10)]. For most common liquids, $\alpha < 0$, so that the surface flow is from hot to cold. In the smectic films flow is from cold to hot where the thermal gradients are at their largest, close to the lateral edges of the holder. However, for the smectic phases, it has been shown that $\alpha > 0$ because of enhanced ordering close to the free surfaces [25]. Consequently, thermocapillary flow in the smectic films is from cold to hot.

C. Velocity field

The uniformity in temperature in the central region occurs as a result of the film's thinness and consequent rapid radiative equalization in temperature. We can ignore the thermal contributions to the equations of motion and focus only on the two-dimensional velocity field in the central region. We will not consider any of the forces driving the flow and will develop an empirical model of the velocity field. The model will then be used to solve the equation for the director field.

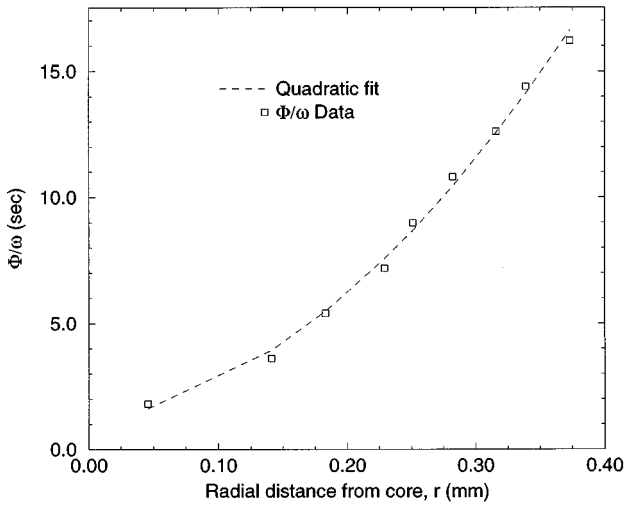

FIG. 12. Variation of the director phase divided by the local angular velocity, Φ/ω, as a function of r in the ring flow regime along a cross section through the vortex.

The fluid in the vortices moves around the vortex with an angular velocity $\omega(r,\theta)$. To determine the properties of $\omega(r,\theta)$, tangential velocities of flow as a function of r and θ were measured. In each vortex, $\theta = 0$ corresponds to the direction to the closest differentially heated wall. The radial dependence of the velocity v_θ of the flow along the $\theta = 0$ line is given in Fig. 6. In the range $r = 0.25 - 1.00$ mm from the center of rotation, $v_\theta = mr + b$, where m represents the angular velocity. Nonzero b represents the uncertainty in the center of rotation. Similar plots of v_θ vs r are shown for another film in Fig. 7, which includes both data along the $\theta = 0$ line as in Fig. 6 and along a radial line at 110°. The results shown in Fig. 7 indicate this constancy of $\omega(r)$ is a general property of the flow, even though it does vary significantly with θ.

The dependence of ω on θ can be understood by realizing that a rectangular film holder does not exhibit cylindrical symmetry. The edges of the film holder place constraints on the rotation of the fluid. The distance R from the center of the vortex to the film-holder boundaries changes with θ. Consequently, the cross-sectional area of the film, defined as Rt (t is the thickness of the film), also depends on θ. In order for the mass flux through these cross sections to be conserved, the angular velocity must vary as well. Using this conservation of mass flux argument, the angular velocity around the film should scale as

$$\omega(\theta) = \frac{R_0^2}{R^2(\theta)}\omega_0, \tag{16}$$

where R_0 and ω_0 are, respectively, the radial distance and the angular velocity at the $\theta = 0$ line connecting the vortex center to the film-holder edge.

The plot of ω vs θ for one film is shown in Fig. 8. Also in the figure is the expected profile, given the maximum angular velocity in the vortex, when the angular velocity is rescaled according to Eq. (16). In order to obtain the profile, Eq. (16) was matched to the data at two points, at $\theta = 0$ and at $\theta = \pi$. Qualitatively, the angular velocity is seen to agree

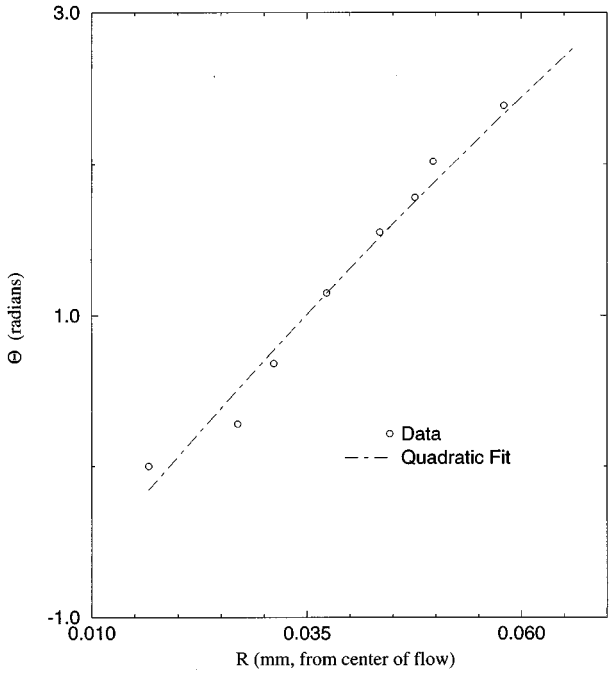

FIG. 13. Spiral structure, θ vs r. Dashed line indicates quadratic fit to the data. Film of 81 layers in a gradient of 78.9 °C − 77.8 °C.

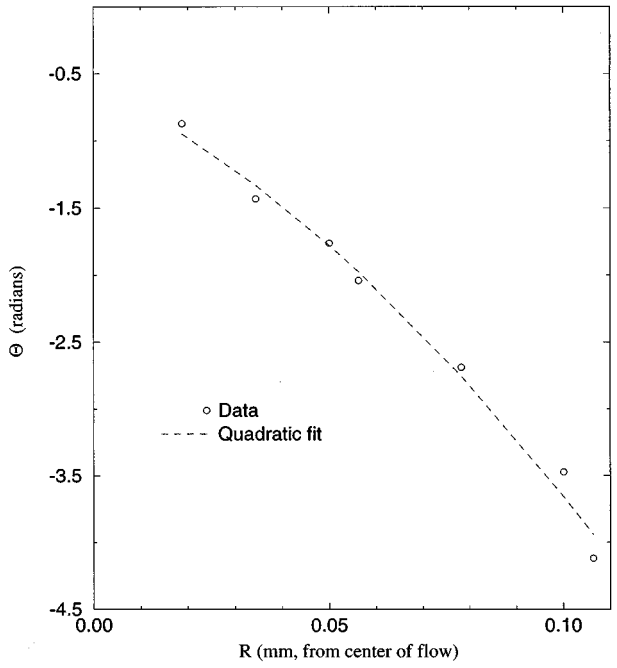

FIG. 14. Antispiral structure, θ vs r. Dashed line indicates quadratic fit to the data. Film of 140 layers in a gradient of 81.3 °C − 79.7 °C.

with the predicted angular velocity. This would suggest that the motion of the liquid crystal corresponds to rigid body flow in θ, but not in r, due to the presence of fixed and soft boundaries. The fluid experiences dilatational expansions and contractions in r as a function of θ. These dilatational motions lead to a variation in the angular velocity in order to conserve the mass flux across any given cross section of the film.

D. Director field

As a first approximation, we assume cylindrical symmetry of the velocity field. This is justified by the measured velocity field, after the coordinates are rescaled to account for the actual rectangular film shape. The velocity field is assumed to depend on r and to have a component in the $\hat{\theta}$ direction only, $\vec{v}=(0,v_\theta)$, where (r,θ) are measured from the center of the vortex motion. The magnitude of v_θ may then be expressed in terms of the local angular velocity of the ''background'' fluid, $\omega(r)$, with $v_\theta=r\omega(r)$ [15]. The form for the velocity field can then be used to find an analytic solution to Eq. (13).

If ω is constant, so that the flow of the fluid approximates that of a rotating rigid body, then $v_\theta=r\omega$. For a static distortion, the orientation field in the vicinity of the disclination is given by $\Phi=s\theta+C$, where C is a constant and s is the topological charge for the point disclination [13]. A radial dependence is introduced as a result of the constraints imposed by the boundary conditions on the flow and orientation fields. We therefore replace C with the radial dependence $f(r)$, where $f(r)$ is subject to the flow's initial conditions and the film's boundary conditions. Therefore Φ is assumed to have a solution of the form $\Phi=s\theta+f(r)$, where the constant term C has been replaced with a function of the radius measured from the center of the flow. The flow is thus assumed to distort the static pattern of the $\hat{c}$ field in the radial direction only. Equation (13) then simplifies to

$$\frac{df}{dr}+r\frac{d^2f}{dr^2}=\frac{2\lambda_1}{k}\omega. \tag{17}$$

Using polar coordinates, this may be readily integrated to give a solution for Φ of the form

$$\Phi=\frac{\lambda_1}{k}\omega r^2+Ar+B+s\theta. \tag{18}$$

TABLE I. Average orientational diffusion constant for Sm-C films extracted from the Schlieren pattern for films with no disclinations present — creating a ring pattern.

Film number	Film thickness (in layers)	Avg. temp. (°C)	Diffusion constant (10^{-2} mm^2/s)
1	3	76	1.47
	3	76	2.37
	3	76	4.41
2	100	76	1.08
	100	76	1.11
	100	76	1.94
3	126	80.5	1.11
4	140	81.5	1.08
	140	81.5	1.39
	140	80.5	1.01
	140	81.0	1.02

TABLE II. Average orientational diffusion constant for Sm-*C* films extracted from the Schlieren pattern for films with disclinations present — creating a spiral pattern.

Disclination strength	Film thickness (in layers)	Avg. temp. (°C)	Diffusion constant (10^{-2} mm^2/s)
+1	100	76.5	0.24
	3	76.0	14.1
	140	81.5	0.651
−1	140	81.5	0.982
		78.4	1.24
	140	81.0	1.75

A and B are constants of integration and will be determined by the boundary conditions on Φ and r. This result may also be written as

$$\frac{\Phi-\Phi_0}{\omega}=\frac{\lambda_1}{k}(r-r_0)^2+s\theta, \tag{19}$$

where Φ_0 and r_0 are constants of the integration.

One readily sees that for $s=0,+1,-1$, there are three possible solutions to Eq. (19) for regions of equal phase, $\Phi=$ const. For $s=0$, the director field will form rings of equal phase. For $s=\pm 1$, the director will form spiraling arms of equal phase that will spiral outward from the center of rotation either with or against the sense of rotation of the angular velocity. (See Figs. 9–11.)

Figure 9 is a video image of the ring flow pattern for a 120 layer thick DOBAMBC film in the Sm-*C* phase. The schematic below the image illustrates the orientation field and flow direction in the vicinity of the point disclination. This film was suspended on a 6:1 aspect ratio film holder with an applied gradient of 1.56 °C/cm, with the hot side held at 81.25 °C. Only a portion of the flow vortex could be visualized at any given time, though the entire film could be illuminated with the laser at once.

The observed ring pattern followed the streamlines of the flow in terms of the overall cellular pattern of the vortex structure and the location of the vortex center in the absence of point disclinations or dust particles. The presence of a ring structure in the Schlieren texture in the two-dimensional cellular flow in which there are no point disclinations present exemplifies the $s=0$ solution. The flow is not axially symmetric due to the presence of the rectangular no-slip boundary conditions on the film's edges. Consequently, the director field will likewise not be axially symmetric, but will be constrained to follow the geometry of the streamlines.

If the liquid crystal is strongly anchored on the film edges, with homeotropic boundary conditions, it is expected that the orientation of the $\hat{c}$ director will be perpendicular with respect to the edges of the film holder. These boundary conditions impose on the film a net topological charge of $+1$ in order to accommodate the $+2\pi$ rotation of the orientation field around the film's edge. In order to conserve this topological charge, if one vortex contains a $+1$ defect the other must contain a net topological charge of zero, assuming no other disclinations occur on the film. It will be shown that a region of zero topological charge exhibits ring flow under an applied thermal gradient, thus the flow-alignment and ring flow regimes may be seen in conjunction with each other.

The parameter λ_1/k is the only material constant appearing in the equation, and is the inverse of the diffusion constant for the orientation field. The topological strength s of the disclinations present on the film is set by the initial and boundary conditions at the start of the flow. These two parameters (λ_1/k and s) will completely characterize the flow-orientation coupling and the emergent patterns in the orientation field with the application of an angular velocity ω to the film.

The elastic constant k was assumed to be isotropic, that is, the bend and splay elastic constants were assumed to be equal in magnitude. For DOBAMBC, there is a factor of 6 difference between the two elastic constants in thin films [1,14,25,27]. The unequal magnitude between k_{11} and k_{33} does not affect the sensitivity of the patterns emerging in the flow-orientation field to the initial conditions. It will affect the local spatial expression of the pattern, as bend distortions will be favored over splay distortions. The difference appears as a modulation in a brush's width as it is wound around the point disclination by the flow.

From Eq. (18), if the angular velocity ω is known, the diffusion constant k/λ_1, may be determined. Equation (18) was found assuming that ω was constant throughout the flow region. Nonetheless, if ω is a function of θ, it will not affect the analysis following Eq. (13). Thus we may replace ω with $\omega(\theta)$ in Eq. (18).

The diffusion constant can be extracted from the data for the ring flow regime by plotting the position of the dark bands in the rings versus Φ/ω for a fixed polar angle θ. The value of angular velocity $\omega(\theta)$ is unchanging as all measurements are done along a single radial line with θ fixed; for example, all measurements would be done along the linear portion of the plot in Fig. 6. An example of this measurement is illustrated in Fig. 12. The dashed line in Fig. 12 is fitted to a quadratic form. The coefficient λ_1/k extracted from this fit is the inverse of the constant. Using the measured angular velocity, the extracted diffusion constant for various films of about the same thickness and showing ring flow at different rescaled angular velocities is summarized in Table I.

In Table I the ''Film number'' corresponds to the film on which the flow was induced. Typically, several measurements were done on one film. In films 2–4, the thermal gradients that produced the flow were induced by using TEDs on each side of the film holder. Dust particles or other inhomogeneities on the film surface were used to measure the velocity of the flow. The diffusion constant was extracted using the method discussed above. For films 2–4, the average diffusion constant is 1.22×10^{-2} mm^2/s, with a standard deviation of $\pm0.31\times10^{-2}$ mm^2/s.

In film 1, the film's thinness did not allow dust motes to collect on the film's surface. The motion was induced using the Gaussian profile of the illuminating laser beam to establish the thermal gradients on the edge of the holder. The velocity was initially measured by observing the motion of the point disclination in the vortex before it settled in the center of the vortex. This angular velocity was then used for all three runs listed. However, the thermal gradient was in-

creased between each run. The increase in gradient probably led to an increase in the angular velocity, which could not be measured. The increase in ω would lead to an apparent increase in the diffusion constant. These data were included as they suggest that the diffusion constant for the thin films is not very different from that of the other relatively thick films.

Figures 10 and 11 are photographs of the two regimes we have labeled ''spiral'' and ''antispiral.'' For a $+1$ defect in the center of the flow, the arms of the defect in the Schlieren texture are expected to spiral inward when following a region of constant phase, $\Phi=\Phi_0$, around the defect in the same sense as the rotation of the angular velocity, ω. For a -1 defect, we expect an outward spiraling of the texture with ω. The photographs display both of these relationships. The defect strengths in the centers of the vortices were determined to be, respectively, $s=+1$ and -1 for each pattern. Thus the predicted mediation of the $\hat{\hat{c}}$-director field pattern by the defect in the center of the flow is obviously brought to bear in these observations.

The spirals are not quadratic in form, as would be expected from the theory. Again, the angular velocity ω depends on the polar angle θ. Using Eq. (19) so that the angular and radial dependencies are on opposite sides of the equation, we can write

$$\frac{\Phi_0 - s\theta}{\omega(\theta)} = \frac{\lambda_1}{k}(r-r_0)^2. \tag{20}$$

Thus, from a quadratic least squares fit applied to a plot of θ/ω vs r, we should be able to extract the diffusion constant $(\lambda_1/k)^{-1}$ for spiral flows. The sign of the extracted coefficient will distinguish the topological charges from each other. Graphs of θ/ω vs r are given in Figs. 13 and 14 for the two separate flows. The diffusion constants extracted from quadratic fits are listed in Table II. The diffusion constant for thin films of DOBAMBC in other temperature ranges has been obtained using the rate of collapse of a ring [7], and through the use of cross-correlation intensity-fluctuation spectroscopy [14]. The ring collapse experiment shows a decrease in the diffusion constant with thickness, with its value dropping from 9.2×10^{-3} mm^{-2}/s in a two layer film to 5.0×10^{-3} mm^{-2}/s for a five layer film [7]. Van Winkle and Clark distinquish between the splay and bend diffusion constants, and shows that the splay diffusion varies from 7.0 to 25.0 in units of 10^{-3} mm^{-2}/s over a temperature range of 66–105 °C [14]. The bend diffusion constant was about a factor of 6 smaller than the splay constant in their data. Our results are self-consistent and are also consistent with those prior results.

The diffusion constant extracted for the flow around the $s=+1$ disclination are not self-consistent, nor consistent with the $s=-1$ or $s=0$ data. It seems that the simple theory described by Eq. (16) does not provide a complete model for the flow around the $+1$ defect. This may be due to the qualitative differences between the orientation field surrounding the $s=+1$ defects compared with other patterns. For all patterns, except around the $s=+1$, as the defect is encircled around in a closed path the angle between the flow streamline and the director varies continuously between 0 and 2π. For the $s=+1$ defect, closed paths can be found where the angle between the flow streamline and the director remains constant. This constant angle will vary with distance from the disclination core. The $s=0$ and $s=-1$ cases involve flow streamlines intersecting the director field at many angles, thus the viscoelastic response measured will be an average at any radius. The $s=+1$ case involves distinguishable flows relative to the director, thus the viscoelastic response may vary significantly as a function of r.

V. SUMMARY

We have created flows in FSLCFs using surface-tension gradients. These flows, when the angular velocity is appropriately rescaled to take into account mass conservation, are seen to be to a good approximation equivalent to ''rigid body'' rotational flows with a dilatational component.

The effect of a point disclination on the pattern that develops in the director field when subjected to a shearing flow in a FSLCF has been seen. By assuming a simple profile for the velocity field, a model for the spatial dependence of the director phase, Φ, has been developed. The observations of the patterns that develop are consistent with the defect mediation that our model predicts.

By replacing the angular velocity ω with our measured angular velocity $\omega(\theta)$, as suggested by the rescaling argument for the rigid body flow with dilatational motion, we were able to extract a diffusion constant for our material. The data for the 0 and -1 disclination mediated flows were seen to be consistent with each other and with the results of other researchers. The $+1$ disclinations, however, did not give consistent results. We attribute this to the geometry of the molecular orientation field with respect to the flow direction. The coupling may play a larger role in the $+1$ disclination case because of the relative geometry between the molecules and the flow is unchanging in the $+1$ case, unlike the -1 and 0 cases.

[1] C.Y. Young, R. Pindak, N.A. Clark, and R.B. Meyer, Phys. Rev. Lett. **40**, 773 (1978); C. Rosenblatt, R. Pindak, N.A. Clark, and R.B. Meyer, *ibid.* **42**, 1220 (1979).

[2] E.I. Katz and V.V. Lebedev, Kristallografiya **31**, 23 (1986) [Sov. Phys. Crystallogr. **31**, 10 (1986)]; **33**, 687 (1988) [**33**, 404 (1988)].

[3] P.C. Martin, P.S. Pershan, J. Swift, and Phys. Rev. Lett. **25**, 844 (1970).

[4] D. Forster, T.C. Lubensky, P.C. Martin, J. Swift, and P.S. Pershan, Phys. Rev. Lett. **26**, 1016 (1971); P.C. Martin, O. Parodi, and P.S. Pershan, Phys. Rev. A **6**, 2401 (1972).

[5] S.W. Morris, J.R. de Bryun, and A.D. May, Phys. Rev. A **44**, 8146 (1991).
[6] P.E. Cladis, Y. Couder, and H.R. Brand, Phys. Rev. Lett. **55**, 2945 (1985).
[7] R. Pindak, C.Y. Young, R.B. Meyer, and N.A. Clark, Phys. Rev. Lett. **45**, 1193 (1980).
[8] R.B. Meyer, L. Liebert, L. Strzelecki, and P. Keller, J. Phys. (Paris) Lett. **36**, L-69 (1975).
[9] F. Bloisi, L. Vicari, P. Cavaliere, S. Martellucci, J. Quartieri, P. Mormile, and G. Pierattini, Appl. Phys. B **47**, 67 (1988).
[10] P. Manneville, *Dissipative Structures and Weak Turbulence* (Academic Press Inc., Boston, 1990).
[11] H. Pleiner, Liq. Cryst. **3**, 249 (1987).
[12] P.G. de Gennes, *The Physics of Liquid Crystals* (Oxford Press, London, 1974); W.W. Beens and W.H. de Jeu, J. Chem. Phys. **82**, 3841 (1983); H. Kneppe and F. Schneider, Mol. Cryst. Liq. Cryst. **65**, 23 (1981).
[13] S. Chandrasekehar, *Liquid Crystals*, 2nd ed. (Cambridge University Press, Cambridge, England, 1992).
[14] D.H. Van Winkle and N.A. Clark, Phys. Rev. A **38**, 1573 (1988).
[15] L.D. Landau and E.M. Lifshitz, *Fluid Mechanics* (Addison-Wesley, Reading, MA, 1959).
[16] W. Helfrich, Phys. Rev. Lett. **23**, 372 (1969).
[17] E.I. Katz and V.V. Lebedev, J. Phys. (Paris) **46**, 2093 (1985).
[18] A. Bottger and J.G.H. Joosten, Europhys. Lett. **4**, 1297 (1987).
[19] C.Y. Young and N.A. Clark, J. Chem. Phys. **74**, 4171 (1981).
[20] P.G. de Gennes, Phys. Fluids **17**, 1645 (1974).
[21] V.G. Levich and V.S. Krylov, Annu. Rev. Fluid Mech. **1**, 293 (1969).
[22] R. Siegel and J.R. Howell, *Thermal Radiation Heat Transfer*, 3rd ed. (Hemisphere Publishing Corp., Washington, DC, 1992).
[23] S.H. Davis, Annu. Rev. Fluid Mech. **19**, 403 (1987).
[24] K. Miyano, Phys. Rev. A **26**, 1820 (1982).
[25] A. Ferguson and S.J. Kennedy, Philos. Mag. **26**, 41 (1938); S. Krishnaswamy and R. Shashidhar, Pramana Suppl. **1**, 247 (1975); Mol. Cryst. Liq. Cryst. **38**, 353 (1977); C.A. Croxton, *Statistical Mechanics of the Liquid Surface* (Wiley, New York, 1980).
[26] P. Pieranski *et al.*, Physica A **194**, 364 (1993).
[27] C. Rosenblatt, R.B. Meyer, R. Pindak, and N.A. Clark, Phys. Rev. A **21**, 140 (1980).